CHEMISTRY OF MATERIALS
Article

Chem. Mater. **2010,** *22,* 4867–4878 4867
DOI:10.1021/cm903793u

Atomic Layer Deposition of Ru/RuO_2 Thin Films Studied by In situ Infrared Spectroscopy

S. K. Park,[†] R. Kanjolia,[‡] J. Anthis,[‡] R. Odedra,[‡] N. Boag,[§] L. Wielunski,[∥] and Y. J. Chabal*[,†]

[†]*Materials Science and Engineering Department, University of Texas at Dallas, Richardson, Texas 75080,* [‡]*SAFC Hitech, Haverhill, Massachusetts 01832,* [§]*Functional Materials, Institute for Materials Research, University of Salford, Manchester M5 4WT, United Kingdom, and* [∥]*Department of Physics and Astronomy, Rutgers University, Piscataway, New Jersey 08854*

Received December 17, 2009. Revised Manuscript Received July 5, 2010

The deposition of ruthenium thin films is investigated using a newly synthesized precursor (cyclopentadienyl ethylruthenium dicarbonyl, $Ru(Cp)(CO)_2Et$) and O_2 gas as reactants. The conditions to achieve self-terminated surface reactions (sample temperature, precursor pulse length and precursor gas pressure) are investigated and the resulting composition, conductivity, and surface morphology are determined during/after deposition on hydrogen-terminated silicon (111) surfaces using in situ FTIR, and ex situ Rutherford back scattering, X-ray photoelectron spectroscopy, and atomic force microscopy. Higher growth rates (~1.5−3 Å) are obtained compared to those typical of ALD of metals (~0.5−1 Å), under conditions of saturation, i.e., through self-terminated surface reactions. Infrared absorption measurements reveal that bridged CO formed by the self-reaction of $Ru(Cp)(CO)_2Et$ leads to surface passivation, thus terminating the precursor self-reaction. They also show that, under these "saturation" growth conditions, metallic Ru develops during the early stage of deposition (1−5 cycles), and RuO_2 is observed later in the growth. The deposition rate is linear with cycles after an initially slow nucleation stage and the film becomes metallic after ~22 cycles. Thick films (~45 nm) grown with short pulses produce metallic polycrystalline ruthenium with hcp structure.

1. Introduction

Ruthenium and ruthenium oxides remain chemically stable in contact with high-κ dielectric such as hafnium oxide and aluminum oxide, even at high temperatures.[1] Additionally, they have relatively high work functions.[2] Furthermore, ruthenium dioxide (RuO_2) is a conductive material in spite of its oxide character.[3] Both Ru and RuO_2 are being considered as seed layer for copper deposition, which is important for interconnections in microelectronics, capacitor electrodes for memory devices, and gate metal for metal-oxide-semiconductor field-effect transistors.[1,4−9] There have therefore been increased efforts to study the deposition of Ru and/or RuO_2 prepared by a variety of growth techniques.[2,10−12] Recent precursors developed for Ru and RuO_2 deposition have been: $Ru(Cp)_2$,[1,13−15] $Ru(EtCp)_2$,[2,4,7,16] Ru(EtCp)(2,4-dimethylpentadienyl),[17,18] $Ru(thd)_3$ (thd = 2,2,6,6-tetramethyl-3,5-heptanedione)[9] and *N*,*N*-Dimethyl-1-ruthenocenylethylamine[19] for atomic layer deposition (ALD) and for chemical vapor deposition (CVD).[5,6,8,10,11,20−25]

*Corresponding author. E-mail: chabal@utdallas.edu.

(1) Papadatos, F.; Spyridon, S.; Zubin, P.; Steven, C.; Eric, E. *Mater. Res. Soc. Symp. Proc.* **2002**, *716*, B2.4.1–B.2.4.5.
(2) Aaltonen, T.; Al, P.; Ritala, M.; Leskel, M. *Chem. Vap. Deposition* **2003**, *9*(1), 45–49.
(3) Kadoshima, M.; Aminaka, T.; Kurosawa, E.; Aoyama, T.; Nara, Y.; Ohji, Y. *Jpn. J. Phys.* **2008**, *47*(4), 2108–2111.
(4) Kwon, O.-K.; Kwon, S.-H.; Park, H.-S.; Kang, S.-W. *J. Electrochem. Soc.* **2004**, *151*(12), C753–C756.
(5) Kwon, O.-K.; Kim, J.-H.; Park, H.-S.; Kang, S.-W. *J. Electrochem. Soc.* **2004**, *151*(2), G109–G112.
(6) Tomonori, A.; Masahiro, K.; Soichi, Y.; Kazuhiro, E. *Jpn. J. Phys.* **1999**, *38*(4B), 2194–2199.
(7) Kang, S. Y.; Choi, K. H.; Lee, S. K.; Hwang, C. S.; Kim, H. J. *J. Electrochem. Soc.* **2000**, *147*(3), 1161–1167.
(8) Yim, S.-S.; Lee, D.-J.; Kim, K.-S.; Lee, M.-S.; Kim, S.-H.; Kim, K.-B. *Electrochem. Solid-State Lett.* **2008**, *11*(9), K89–K92.
(9) Kang, S. Y.; Hwang, C. S.; Kim, H. J. *J. Electrochem. Soc.* **2005**, *152*(1), C15–C19.
(10) Aaltonen, T.; Ritala, M.; Arstila, K.; Keinonen, J.; Leskel, M. *Chem. Vap. Deposition* **2004**, *10*(4), 215–219.
(11) Lai, Y.-H.; Chen, Y.-L.; Chi, Y.; Liu, C.-S.; Carty, A. J.; Peng, S.-M.; Lee, G.-H. *J. Mater. Chem.* **2003**, *13*(8), 1999–2006.
(12) Park, S.-E.; Kim, H.-M.; Kim, K.-B.; Min, S.-H. *Thin Solid Films* **1999**, *341*, 52–54.
(13) Aaltonen, T.; Rahtu, A.; Ritala, M.; Leskela, M. *Electrochem. Solid-State Lett.* **2003**, *6*(9), C130–C133.
(14) Park, K. J.; Terry, D. B.; Stewart, S. M.; Parsons, G. N. *Langmuir* **2007**, *23*(11), 6106–6112.
(15) Park, K. J.; Doub, J. M.; Gougousi, T.; Parsons, G. N. *Appl. Phys. Lett.* **2005**, *86*(5), 051903–3.
(16) Kwon, S.-H.; Kwon, O.-K.; Kim, J.-H.; Jeong, S.-J.; Kim, S.-W.; Kang, S.-W. *J. Electrochem. Soc.* **2007**, *154*(9), H773–H777.
(17) Kim, S. K.; Lee, S. Y.; Lee, S. W.; Hwang, G. W.; Hwang, C. S.; Lee, J. W.; Jeong, J. *J. Electrochem. Soc.* **2007**, *154*(2), D95–D101.
(18) Heo, J.; Lee, S. Y.; Eom, D.; Hwang, C. S.; Kim, H. J. *Electrochem. Solid-State Lett.* **2008**, *11*(2), G5–G8.
(19) Kukli, K.; Ritala, M.; M., K.; Leskel, M. *J. Electrochem. Soc.* **2010**, *157*(1), D35–D40.
(20) Cheng, W.-Y.; Hong, L.-S.; Jiang, J.-C.; Chi, Y.; Lin, C.-C. *Thin Solid Films* **2005**, *483*(1−2), 31–37.
(21) Matsui, Y.; Hiratani, M.; Nabatame, T.; Shimamoto, Y.; Kimura, S. *Electrochem. Solid-State Lett.* **2001**, *4*(2), C9–C12.
(22) Tian, H.-Y.; Chan, H.-L.-W.; Choy, C.-L.; Choi, J.-W.; No, K.-S. *Mater. Chem. Phys.* **2005**, *93*(1), 142–148.
(23) Matsui, Y.; Hiratani, M.; Nabatame, T.; Shimamoto, Y.; Kimura, S. *Electrochem. Solid-State Lett.* **2002**, *5*(1), C18–C21.
(24) Tomonori, A.; Kazuhiro, E. *Jpn. J. Phys.* **1999**, *38*(10A), L1134–L1136.
(25) Kim, B. S.; Kang, S. Y.; Seo, H. S.; Hwang, C. S.; Kim, H. J. *Electrochem. Solid-State Lett.* **2007**, *10*(10), D113–D115.

Published on Web 08/11/2010

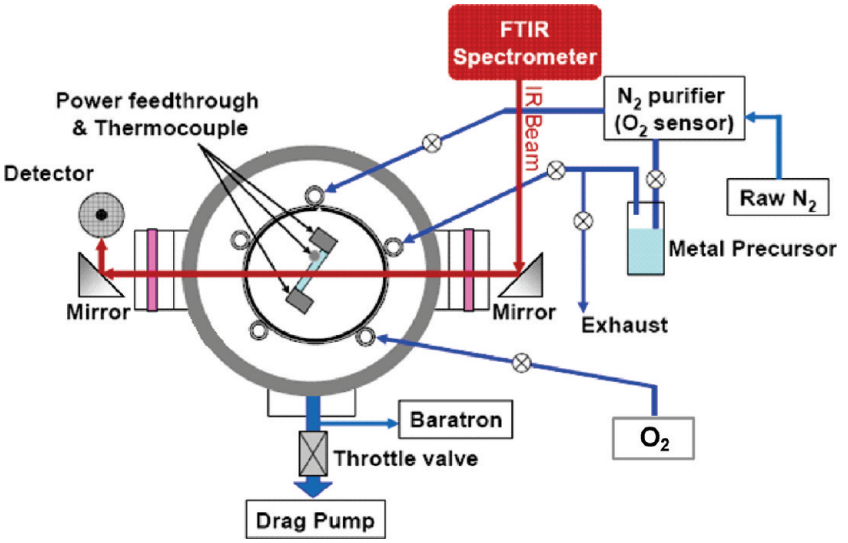

Figure 1. The schematic diagram of ALD reactor connected to FTIR spectrometer for in situ characterization.

In this study, we investigate chemical interactions of cyclopentadienyl ethylruthenium dicarbonyl (Ru(Cp)-$(CO)_2$Et) with H-terminated silicon surfaces during Ru/RuO_2 growth. O_2 is used as the reducing agent, exposed to the surface in alternative pulsing steps. Except for the first 2−3 cycles where low growth rates are observed, we find that the maximum saturation condition through self-reactions of Ru(Cp)$(CO)_2$Et leads to a higher growth rate of metallic Ru/RuO_2 films through ligand exchange. The precursor self-reaction leads to the formation of bridged CO species that passivate the surface, thus terminating the reaction. Oxygen is effective in removing the bridged CO, thus preparing the surface reactive toward the subsequent Ru(Cp)$(CO)_2$Et pulse for further film growth. Under such saturation conditions, atomically controlled growth is possible with a higher growth rate (~1.5 Å). We also compare these ultrathin films with thicker ones grown under conditions more typical of atomic layer deposition (ALD).

Infrared spectroscopy is a useful technique to derive mechanistic information because it can be used in situ, is nondestructive and specific to the chemical nature of surface species and is also sensitive to the electronic response of the metallic film. We combine in situ Fourier transform infrared (FTIR) with ex situ Rutherford backscattering (RBS), X-ray photoemission spectroscopy (XPS), and atomic force microscopy (AFM) to investigate the growth of ruthenium thin films. IR spectroscopy and XPS are particularly useful to examine the intermediate species formed during the growth with this new precursor and O_2 gas as reactants, and to determine the film electronic absorption (i.e., conductivity). RBS is used to measure the coverage of Ru atoms and derive a growth rate, and AFM provides complementary information on the film morphology and uniformity.

2. Experimental Section

In this study, double-side polished, float-zone-grown Si (111) and Si (100) wafers are used. The Si (100) wafers are treated with RCA cleaning followed by deionized water rinsing and N_2 gas drying, to produce clean oxidized surfaces. Atomically flat hydrogen-terminated Si (111) surfaces are prepared by an additional 30 s etching in aqueous HF (~20%) and 2.5 min immersion in NH_4F (~49%) after a standard RCA cleaning, followed by deionized water rinsing and N_2 gas drying.[26] Samples are immediately loaded into a nitrogen-purged reactor. Film growth is performed in a home-built reactor connected to a FT-IR spectrometer (Thermo Nicolet 6700), shown schematically in Figure 1. Ruthenium deposition is performed using a cyclopentadienyl ethylruthenium dicarbonyl [Ru(Cp)$(CO)_2$Et] precursor and O_2 gas as reactants. The ruthenium precursor (produced by SAFC Hitech) is liquid at ambient temperature and kept at ~85 °C, the reactor wall temperature at 70 °C, whereas the Si substrate temperature is varied between 200 and 325 °C. Purified nitrogen gas (O_2 concentration $<1 \times 10^{-5}$ ppm) is used as carrier and purge gas during the process, except for the O_2 pulse. When alternative pulsing is used [Ru precursor and O_2] to grow the films, the process is always started with the Ru pulse (labeled cycle 1/2). A full cycle, labeled by an integer, indicates that an O_2 exposure was performed after the Ru exposure. For instance, cycle $9^1/_2$ indicates that 9 full cycles of Ru + O_2 exposures were performed followed by a Ru exposure.

To reach saturation (described in the Results section), we used an intentionally longer Ru pulse than typical ALD conditions. As the purging N_2 is turned off, the throttle valve between the chamber and the vacuum pump (Drytel 1025C) is closed to 1% of its open setting and a 5 s pulse of Ru(Cp)$(CO)_2$Et is introduced with N_2 carrier gas (100 sccm). After the 5 s pulsing, the throttle valve is closed completely for a period of 25 s. The throttle valve is reopened fully and 500 sccm N_2 purge established for 5 min (0.9 Torr). The following O_2 pulse is established by a 2 s pulse (100 sccm, 0.4 Torr) with N_2 purge turned off and throttle valve fully open. Another purge cycle of 5 min (500 sccm, 0.9 Torr) is then performed before the next Ru precursor dosing. The unusual procedure of the extra 25 s residence time for the Ru precursor (i.e., with no pumping) is to achieve full saturation at a sample temperature most favorable to ALD growth (~300 °C) without depleting the Ru precursor at an unsustainable rate. Because the H/Si surface is

(26) Higashi, G. S.; Chabal, Y. J.; Trucks, G. W.; Raghavachari, K. *Appl. Phys. Lett.* **1990**, *56*(7), 656–658.

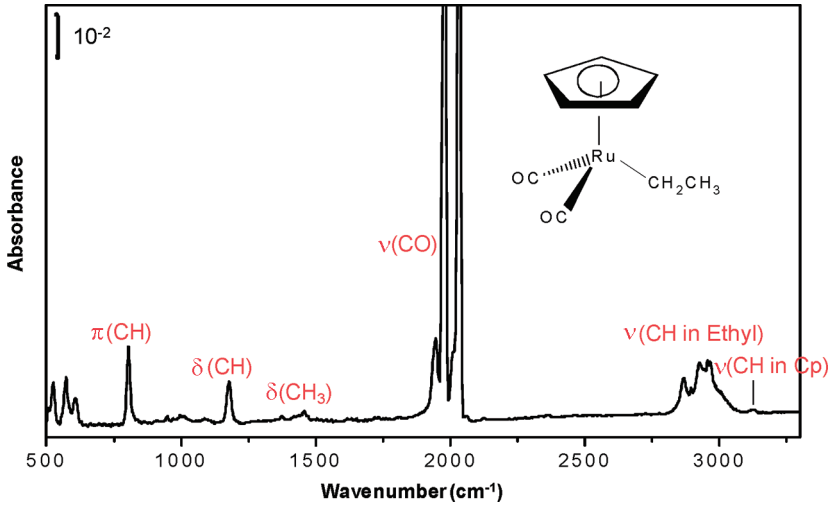

Figure 2. IR absorption spectrum of gas phase $Ru(Cp)(CO)_2Et$ (source temperature 85 °C) at 0.20 Torr.

inert to O_2 (or H_2O) at 300 °C,[27−29] starting with the Ru pulse is appropriate. The long purge time (5 min) is used to prevent cross gas reaction between O_2 and $Ru(Cp)(CO)_2Et$.

The infrared beam is transmitted through the sample at the Brewster angle (single-transmission geometry, 74° incidence angle). The transmitted beam is refocused onto a liquid-nitrogen cooled broadband HgCdTe detector (400−4000 cm^{-1}). The KBr windows for the beam transmission are protected by gate valves during precursor exposures. Rutherford backscattering spectroscopy (RBS) is performed ex situ with 2 MeV He^+ ions at the Rutgers Laboratory for Surface Modification. For the RBS measurements, the detector is positioned for a 160° backscattering angle with respect to the surface normal to measure Ru atom density. A Perkin-Elmer PHI 5600 ESCA System for X-ray photoelectron spectroscopy (XPS) is employed ex situ to characterize the composition of thin films. The photoelectrons are excited using monochromatic Al Kα radiation (1486.6 eV). Survey and detailed spectra are scanned at 45° angle using 1.0 and 0.1 eV step sizes, respectively. A Veeco dimension 3100 atomic force microscope (AFM) is also used to characterize the surface morphology and texture of the deposited Ru films.

3. Results and Discussion

The experimental investigation first focuses on the integrity of the precursor in the reactor chamber and the conditions at which surface reactions can occur in the presence of the precursor. The effort is then to characterize the chemical and electronic properties of the films using primarily IRAS and XPS, and the structure using XRD and AFM.

3.1. Precursor Integrity. As with any ALD study using a new precursor, it is important to determine whether the precursor gases maintain their integrity while in the reactor chamber. To that end, the gas-phase IR spectrum is recorded in the reactor prior to introducing a Si sample in the reactor. The absorption spectrum of the gas phase ruthenium precursor $Ru(Cp)(CO)_2Et$ is measured at 0.2 Torr within 1 s after introduction into the reactor (Figure 2). The gas lines and reactor walls are maintained at 70 °C throughout all measurements. All the vibrational features in the gas phase spectrum can be assigned to vibrational modes of an intact gas phase molecule. Although the metal−ligand vibrations are not directly detectable, the frequencies associated with the carbonyls and Cp ligands are specific to those ligands being attached to a metal atom (Ru). The C−H modes of the Cp ring are at 3120 cm^{-1} (stretching) and at 805 cm^{-1} (ring breathing), the CO groups at 2033, 1978, and 1945 cm^{-1} (the band at 1945 due to ^{13}CO) (CO stretching), and the ethyl groups at 1179 cm^{-1} (C−H bending) and between 2880 and 3000 cm^{-1} (C−H stretching). There is no evidence of additional features in the spectrum, indicating that the Ru precursor gas remains intact (not decomposed) in the reactor when there is no substrate. This is in contrast to previous observations with amidinate precursors in a similar reactor and conditions.[30]

3.2. Growth Conditions. The most important element for film growth is the sample surface temperature. To investigate the temperature at which the Ru precursor can react with the H-terminated Si surface, H/Si (111), the temperature is varied from 200 to 325 °C as no reaction is observed below 200 °C. Above this temperature (200 °C), Figure 3 shows that the intensity of the Si−H stretching mode at 2083 cm^{-1} decreases with its center frequency gradually red-shifting to 2059 cm^{-1}. These observations indicate that the Ru precursor is reacting with atomically flat H/Si (111) surfaces. The Si−H stretch intensity scales with H coverage and its position is sensitive to the environment (dipole coupling and presence of a metallic atom). Perturbation of the initially well-defined Si−H bond array decreases the Si−H/Si-H dipole−dipole coupling by ~10 cm^{-1}, and introduction of Ru atoms into the

(27) Zhang, X.; Garfunkel, E.; Chabal, Y. J.; Christman, S. B.; Chaban, E. E. *Appl. Phys. Lett.* **2001**, *79*(24), 4051–4053.
(28) Zhang, X.; Chabal, Y. J.; Christman, S. B.; Chaban, E. E.; Garfunkel, E. Oxidation of H-covered flat and vicinal Si(111) 1 × 1 surfaces. In *The 47th International Symposium: Vacuum, Thin Films, Surfaces/Interfaces, and Processing NAN06*; Boston, 2001; American Vacuum Society: New York, 2001; pp 1725−1729.
(29) Frank, M. M.; Chabal, Y. J.; Wilk, G. D. *Appl. Phys. Lett.* **2003**, *82*(26), 4758–4760.
(30) Kwon, J.; Dai, M.; Halls, M. D.; Langereis, E.; Chabal, Y. J.; Gordon, R. G. *J. Phys. Chem. C* **2009**, *113*(2), 654–660.

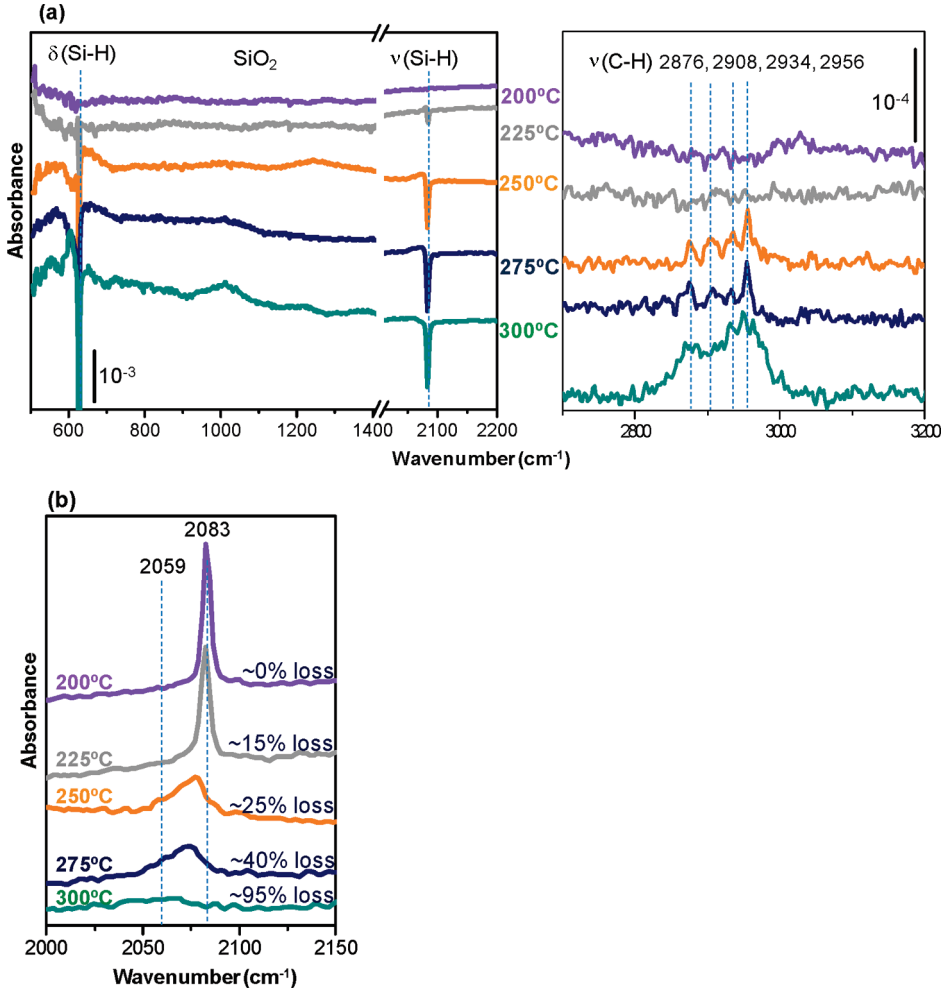

Figure 3. IR absorption spectra of H/Si (111) upon exposure to $Ru(Cp)(CO)_2Et$ as a function of substrate temperature at each 25 °C increment between 200 and 300 °C: (a) referenced to the initial H-terminated Si (111) and (b) referenced to RCA cleaned surface.

vicinity of Si−H bonds further red-shifts the Si−H stretching mode.[31] The presence of chemisorbed Ru precursor is further confirmed by the observation of the vibrational bands associated with its ligands, in C−H stretching region for instance, assigned to its asymmetric CH_3 stretching mode at 2956 cm^{-1}, asymmetric CH_2 stretching mode at 2934 cm^{-1}, symmetric CH_3 stretching mode at 2908 cm^{-1}, and symmetric CH_2 stretching mode at 2876 cm^{-1}. The degree of reaction clearly depends on the substrate temperature. About 40% Si−H layer has reacted after Ru precursor exposure at 275 °C and almost 100% at 300 °C as shown in Figure 3b. Given the large size of the precursor, reaction of 100% of the surface hydrogen indicates that self-reaction or partial decomposition of $Ru(Cp)(CO)_2Et$ takes place.

The choice of precursor exposures longer than typical ALD conditions (~ 5 s pulse +25 s static exposure instead of 1−5 s pulses) is determined by saturation experiments such as shown in Figure 4a. To highlight changes due to continued reaction, we show in Figure 4(i) differential spectra of H/Si(111) exposed to two consecutive $Ru(Cp)(CO)_2Et$ pulses (each one for 5 s exposure with throttle valve only open 1%). The first spectrum shows that most of the surface is reacted (loss of Si−H stretch), the formation of Si−O−Ru (~1000 cm^{-1}), and evidence of ligands from the precursor (Cp modes and CH_x stretch). The spectrum after the second $Ru(Cp)(CO)_2Et$ pulse referenced to that of the first shows only very little additional loss of Si−H, and small perturbation in the spectral regions of the CH_x stretching (2800−3000 cm^{-1}) and Cp (1500−1600 cm^{-1}) region. In fact, there appears to be a very slight loss in these regions, which we will discuss next in the context of the growth by alternative Ru precursor and O_2 pulses.

Over the course of the studies, we found that the most reliable way to achieve saturation for each Ru precursor pulse during growth was to add 25 s static exposure after the 5 s Ru precursor pulse (i.e., with the throttle valve completely closed). That is the procedure that is followed for all the data shown here, except for the last figure. Because the reaction of Ru precursor is saturated, a controlled growth is possible, although it is difficult to establish how complete the saturation is without extensive growth rate studies. As will be shown below, the growth is distinct from ALD because the self-termination mechanism is different. Figure 4(ii) shows differential

(31) Ho, M. T.; Wang, Y.; Brewer, R. T.; Wielunski, L. S.; Chabal, Y. J.; Moumen, N.; Boleslawski, M. *Appl. Phys. Lett.* **2005**, *87*(13), 133103–3.

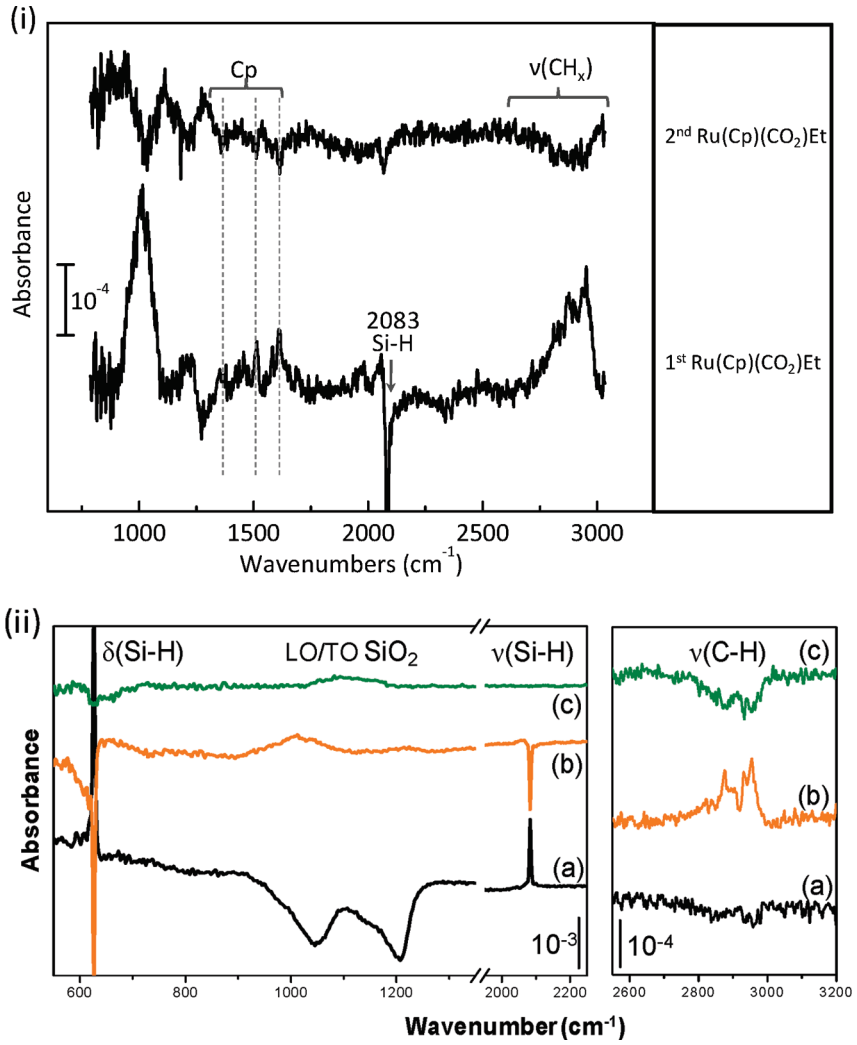

Figure 4. (i) Check for saturation: Differential spectra of H/Si(111) after exposure to Ru(Cp)$(CO)_2$Et for 5 s (+ 25 s static exposure) [1st Ru exposure] and repeating the same treatment [2nd exposure], where each spectrum is referenced to the surface just prior the last exposure. Reactions during the 2nd exposure are negligible. (ii) IR absorption spectra of (a) the initial H/Si(111) surface referenced to an oxide surface, (b) the same surface after the Ru precursor pulse referenced to H/Si(111) [first half cycle], and (c) after O_2 exposure referenced to the previous surface (spectrum b) [second half cycle]. The sample is maintained at 300 °C.

infrared absorbance spectra of H/Si(111) exposed to alternative Ru(Cp)$(CO)_2$Et and O_2 pulses during the first cycle. After the first Ru(Cp)$(CO)_2$Et pulse, which consumes most of H−Si bonds, the surface ethyl group from Ru(Cp)$(CO)_2$Et ligands is removed by the subsequent O_2 pulse. This is consistent with previous work showing that O_2 gas can oxidatively decompose the hydrocarbon ligands of metal precursors during a Ru ALD process,[13] even during the first cycle. Thereafter, it has been suggested that such decomposition involves two steps, with dissociative oxygen adsorption on the noble metal atoms, then facilitating the reaction of oxygen with the ligand.[10,17,21]

Ex situ RBS measurements are particularly useful to determine the absolute coverage of Ru atoms, and therefore to evaluate the average thickness of the grown films, assuming an average Ru atom density. From these data, the growth rate can be extracted as a function of substrate temperature and gas phase conditions. Table 1 shows the temperature dependence for Ru growth. The atomic density of the Ru films deposited in two cycles increases

Table 1. Ru Atom Density As a Function of Temperature on H/Si (111) and Ru Atom Density on SiO_2/Si (100) at 300°C

substrate	temp. (°C)	cycles	Ru atom density (10^{15} atoms/cm^2)
H/Si (111)	250	2	0.05
H/Si (111)	275	2	0.09
H/Si (111)	275	5	0.32
H/Si (111)	300	2	0.33
H/Si (111)	300	3	1.75
H/Si (111)	300	11	10.57
H/Si (111)	300	24	25.20
H/Si (111)	325	5	17.97
SiO_2/Si (100)	*300*	*2*	*0.61*

with temperature: 0.05×10^{15} atoms/cm^2 at 250 °C, 0.09×10^{15} atoms/cm^2 at 275 °C, and 0.33×10^{15} atoms/cm^2 at 300 °C. This indicates that the deposition reactions proceed very slowly below 300 °C. For temperatures higher than 300 °C, the precursor decomposes as evidenced by the RBS results in Table 1. Upon 5 cycles of deposition at 325 °C, the Ru atom density is very large (17.97×10^{15} atoms/cm^2), much higher than expected for ALD growth. Taking the metallic Ru and RuO_2 densities to be 7.27×10^{22} and 3.16×10^{22} atoms/cm^3, this surface

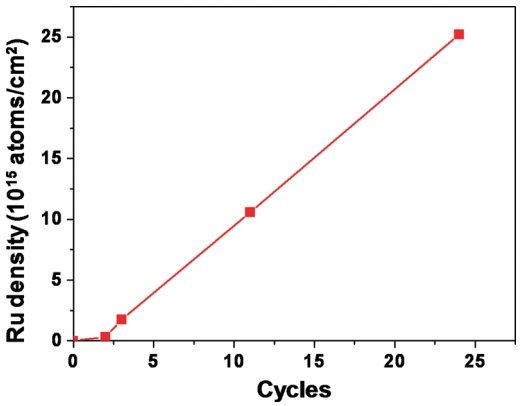

Figure 5. Ru atom density on the number of cycles on H/Si (111) at 300 °C.

density corresponds to about 5.0 Å/cycle (= $0.2 \times 17.97 \times 10^{15}$ atoms/cm^2/7.27×10^{22}atoms/cm^3) to about 11 Å/cycle (= $0.2 \times 17.97 \times 10^{15}$ atoms/cm^2/3.16×10^{22}atoms/cm^3), respectively. There is therefore precursor thermal decomposition at 325 °C.

These data show that a substrate temperature of 300 °C is optimum to reach a controllable growth. At that temperature, the density of Ru atoms is measured by RBS as a function of cycles (Figure 5). For the initial two cycles, the growth rate is very low. However, beyond this initial incubation period, the growth rate increases rapidly and is essentially linear after three cycles. The incubation period below three cycles may be associated with the lack of Ru atom mobility on oxide-free, hydrogen-terminated Si surfaces, as explained below. To explore the role of the oxide substrate, the Ru atom density was measured for films deposited on oxidized silicon wafers, treated only with RCA cleaning and water rinsing. Indeed, on these oxidized surfaces [SiO_2/Si(100)], the Ru atom density of films deposited through two cycles is twice (0.61×10^{15} atoms/cm^2 at 300 °C) than the amount deposited on H/Si surfaces (0.33×10^{15} atoms/cm^2 at 300 °C). These observations are consistent with the fact that metal atoms can diffuse faster on oxide surfaces (i.e., agglomerate), thus leaving a more reactive surface available for further reaction with the metal precursor.[32] Consequently the presence of surface oxygen should be taken into account as an influential factor to initiate the growth of Ru films with this precursor.

3.3. Reaction Mechanism for the Growth of Ru and/or RuO_2 Film. The presence of surface oxygen during the initial two cycles is confirmed using IR absorption spectroscopy by focusing on the spectral region 800 to 1300 cm^{-1} characteristic of Si−O−Si bonds. Figure 6a shows this region for every half cycle of the initial two cycles and also for selected cycles, fifth, tenth, and fifteenth cycle. Interestingly, the absorption of oxides appears after two cycles with weak but visible features in about 1100 cm^{-1} region. After about 5 cycles, the oxide modes split into TO and LO modes, characteristic of a SiO_2 structure. The nature of this oxidation is, however, different from typical (e.g., thermal) SiO_2 films, as can be seen in the spectra over 10 cycles in the 900−1300 cm^{-1} region. We hypothesize that Ru oxide species embedded in the film matrix may be responsible for this observation and the initial formation of this oxide may be facilitated by the presence of Ru at the surface.[33−35]

In the initial stage of growth, the absorption band of Ru=O was not seen markedly. After the first few cycles, stronger modes associated with CO and Ru=O species appear (Figure 6b,c). The growth process seems to be different after the surface is covered with some Ru and possibly Ru oxide. After 5 ALD cycle, the Ru=O vibrational modes appears at ~800 cm^{-1} (for lower oxidation state of Ru) and 830 cm^{-1} (for higher oxidation state of Ru) as expected for the Ru=O stretch mode.[36,37] While the peak centered at 800 cm^{-1} slightly gains intensity upon Ru precursor exposure, the peak at 830 cm^{-1} clearly increases upon O_2 gas exposure. This indicates that a higher oxidation state of Ru is formed, which is expected from an oxidative adsorption and incorporation of oxygen atoms.

The incorporation of oxygen atoms into the Ru metal matrix at certain oxygen coverage (~3 ML) could create subsurface oxygen species between the first and second layer Ru atoms, and could generate those species beneath the second layer due to further penetration. Accordingly, it would produce a metastable surface oxide that fosters the formation of Ru oxide species.[38] This interpretation is based on previous studies where the vibrational spectrum associated with Ru−O bonding in electrochemically deposited RuO_2 system was measured with Raman spectroscopy and reported to have two main features, one in the 470 to 528 cm^{-1} and the other in the 646 to 670 cm^{-1} regions.[39,40] The crystalline RuO_2 showed instead three main features centered at 528, 646, and 716 cm^{-1}.[39,40] The Ru oxide deposited electrochemically to achieve a fully oxidized state was shown by in situ surface enhanced Raman scattering to have two main features at 416 and 710 cm^{-1} as well as a weak broad band near 880 cm^{-1}.[41] Flowing oxygen gas onto the Ru metal layer in the temperature range (250−300 °C) was observed to generate two broad bands near at 800 and 880 cm^{-1} attributed to higher oxidation states of RuO_3 and RuO_4 species, respectively. These species of higher oxidation state in

(32) Dai, M.; Kwon, J.; Halls, M. D.; Gordon, R. G.; Chabal, Y. J. *Langmuir 26*, (6), 3911-3917.

(33) Peden, C. H. F.; Goodman, D. W. *J. Phys. Chem.* **1986**, *90*(7), 1360–1365.
(34) Yongjun, F.; Nicolas, A.-V. *Physica Status Solidi B* **2008**, *245*(9), 1792–1806.
(35) Goodman, D. W.; Peden, C. H. F.; Chen, M. S. *Surf. Sci.* **2007**, *601*(19), L124–L126.
(36) Schoonover, J. R.; Ni, J.; Roecker, L.; White, P. S.; Meyer, T. J. *Inorg. Chem.* **1996**, *35*(20), 5885–5892.
(37) Ferrere, S.; Gregg, B. A. *J. Chem. Soc., Faraday Trans* **1998**, *94*, 2827–2833.
(38) Blume, R.; Niehus, H.; Conrad, H.; Bottcher, A.; Aballe, L.; Gregoratti, L.; Barinov, A.; Kiskinova, M. *J. Phys. Chem. B* **2005**, *109*, 14052–14058.
(39) Mar, S. Y.; Chen, C. S.; Huang, Y. S.; Tiong, K. K. *Appl. Surf. Sci.* **1995**, *90*, 497–504.
(40) Huang, Y. S.; Liao, P. C. *Sol. Energy Mater. Sol. Cells* **1998**, *55*, 179–197.
(41) Mo, Y.; Cai, W.; Dong, J.; Carey, P. R.; Scherson, D. A. *Electrochem. Solid-State Lett.* **2001**, *4*(9), E37–E-38.

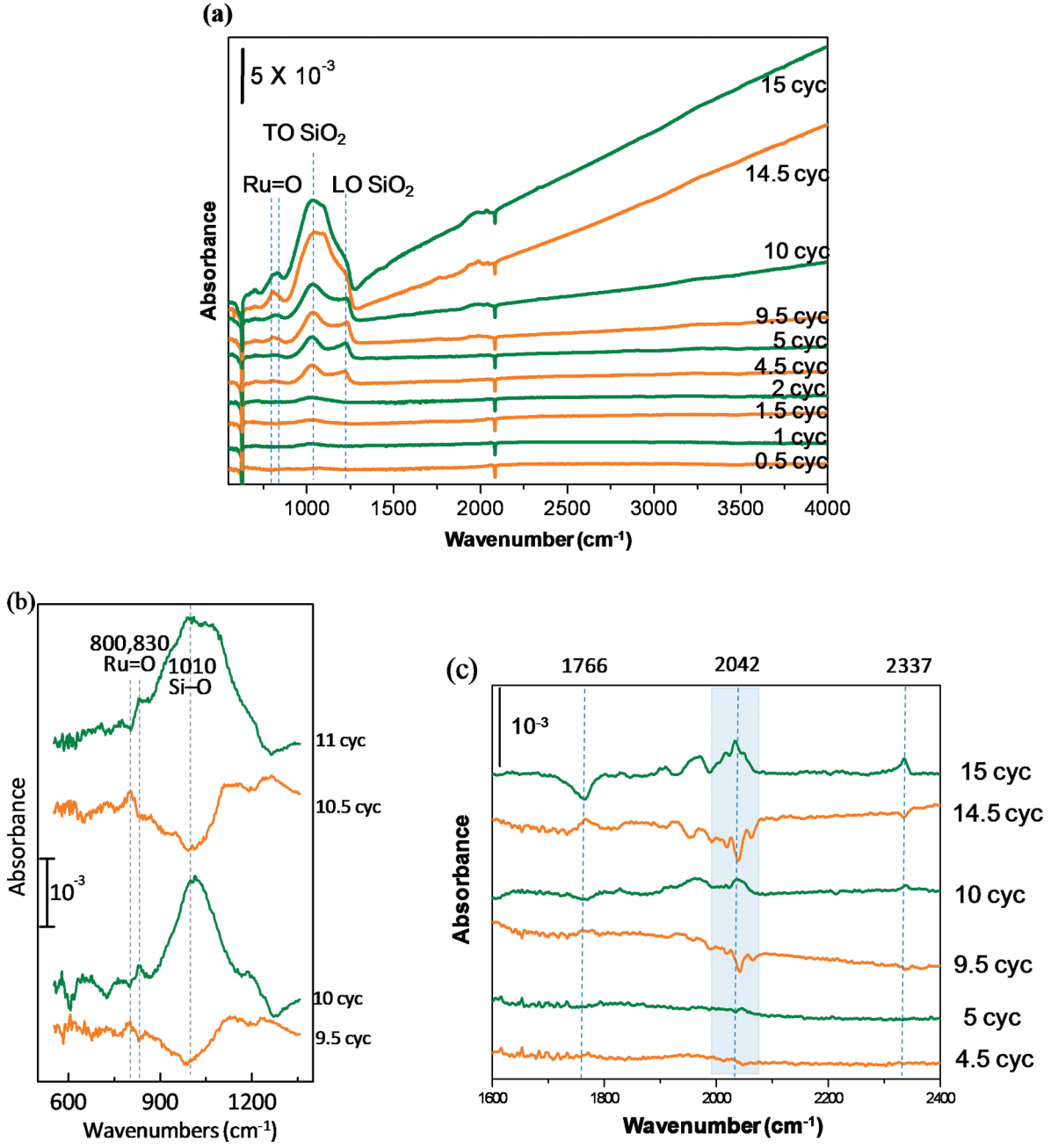

Figure 6. Selected in situ FTIR spectra taken during the first 15 cycles of Ru/RuO_2 deposition on H/Si (111) at 300 °C, referenced to the initial H/Si (111): (a) absorbance over the full spectral range with no baseline correction to show the broadband trends, and (b, c) differential absorption where each spectrum is referenced to the spectrum prior to the last treatment, for two narrow spectral regions. Fractional cycles indicate that exposure to the Ru precursor is done last. Integer cycles indicate that exposure to oxygen is done last. Region b highlights variations in Ru oxide, and region c changes in CO and CO_2 concentrations. Note that the spectra in b are selected from a different run (using identical parameters) from those of a because spurious baseline fluctuations are minimized for this run in this spectral region that is typically difficult to study because of system limitation.

thin film would decompose readily and develop to thermodynamically stable RuO_2 species if left at ambient temperature.[42]

In our system, the growth process is performed at a relatively high reaction temperature (~ 300 °C) with alternative exposure of oxygen gas. The incorporation of oxygen atoms into Ru metal layer appears generate higher oxidation state of Ru oxide as shown a band at 830 cm^{-1} observed during in situ measurements in Figure 6. This value is somewhat lower than that observed at 880 cm^{-1} for surface oxide bonding of RuO_4 species (totally symmetric)[43] obtained by Raman scattering with Ru surface fully oxidized on Au electrodes. Figure 6b shows that the 830 band is induced by the oxygen pulse and is partly removed by the Ru precursor pulse. Eventually, the mode at 830 cm^{-1} grows as a function of cycles as shown in Figure 6a. Therefore, although there is a surface component that reacts with the Ru precursor, there seems to be a steady formation of stable or buried

(42) Chan, H. Y. H.; Takoudis, C. G.; Weaver, M. J. *J. Catal.* **1997**, *172*, 336–345.

(43) Ortner, M. H. *J. Chem. Phys.* **1961**, *34*(2), 556–558.

Ru oxide. Considering the penetration of oxygen atoms into several layers beneath to produce metastable Ru oxides, the higher oxidation states may not be a well-defined single species, but a mixture of multivalent Ru oxides. When the symmetry is broken in the mixture incorporated with oxygen atoms, the Ru−O stretching becomes active but still weak. In contrast to surface-enhanced Raman spectroscopy that is strongly surface sensitive, transmission infrared spectroscopy can detect species that are located below the surface into the bulk. The mode observed at 830 cm^{-1} during O_2 gas exposure may therefore be associated with subsurface oxygen.

Figure 6c displays the stretching vibrational bands of CO and CO_2 species adsorbed on the surface and is referenced to the spectrum prior to the last treatment (i.e., differential spectrum). After the fifth ALD cycle, the CO stretching modes appear in the 1700 to 2100 cm^{-1} range. The band at 1766 cm^{-1} is attributed to bridged CO species, several bands centered at 2042 cm^{-1} to terminal (or linearly bonded) CO species, and weak bands from 1800 to 1950 cm^{-1} to multicoordinated CO species.[44] A distinct band at 2337 cm^{-1} is assigned to terminal (or linearly bonded) CO_2 species.[45] Figure 6a shows that there is an accumulation of CO species in the film, the concentration of which increases as a function of cycles. We focus only on the three major bands associated with bridged CO, terminal CO, and terminal CO_2 because they are clearly observed and spectrally distinct. Among these species, the multicoordinated CO species is expected to be most sensitive to surface heterogeneity. As a result, the modes of multicoordinated CO species are likely to be broadened and more complex over a larger spectral range than those of other CO species.

Figure 6c clearly shows that the bridged CO band at 1766 cm^{-1} gains intensity during exposure to the Ru precursor. However, the peaks at 2042 (terminal CO) and at 2337 cm^{-1} (terminal CO_2) gain intensity upon O_2 gas exposure only in a way that is opposite to what happens during the Ru precursor exposure. These observations indicate that during Ru precursor exposure the terminal CO and terminal CO_2 species are removed, while a bridged CO species appears. This bridged CO passivates the surface, thus terminating the self-reaction of the precursor.

During the O_2 gas pulse, O_2 activates the surface again by removing the bridged CO and forming terminal CO and CO_2 species. These terminal CO and CO_2 may be involved in the subsequent reaction of the Ru precursor. On the basis of the infrared spectra, the surface reaction can be summarized as activation through terminal CO and CO_2 formation after O_2 and termination of reaction through bridged CO formation after $Ru(Cp)(CO)_2Et$ pulses.

Transition metal carbonyl clusters can coordinate with CO species in various ways, to form terminal, bridged, face-capped or mixed species.[46] When the cluster is small or flat, terminal CO species are mostly formed because the binding energy of bridged CO is calculated to be less than that of terminal CO species.[47] However, when the clusters become larger and more complex, bridged CO and/or face capping CO species (≡C−O) are preferentially formed and constitute the dominant ligands. When the deposition of Ru/Ru oxide film is carried out progressively, the morphology of the layer becomes more complex and more similar to large and complex clusters. Accordingly, the bridged CO species are formed preferentially, rather than terminal CO species, and appear stable. In particular, bridged CO species anchored on the surface do not react with the Ru precursor. Therefore, the bridged CO species act as a reaction quencher, terminating the deposition reactions. The growing coverage of bridged CO species during Ru precursor exposure hinders the self-reaction of the Ru precursor on the surface and therefore terminates the film growth. In contrast, the terminal CO possesses a triple bond (one σ bond and two π bonds); the π bond makes it possible to react with the Ru precursor, eventually leading to the formation of bridged CO species. As the Ru/Ru oxide system induces a catalytic oxidation[48] to convert adsorbed CO to CO_2 species, there is a kinetic competition process between the bridged CO and the terminal CO/CO_2 species. When the generation of bridged CO species dominates over that of terminal species, the deposition process terminates. The terminal CO_2 species can be desorbed much more easily, leaving reactive sites for Ru atoms that promote further film growth.

Oxygen gas behaves as an activator because it can convert the bridged CO species to terminal CO and terminal CO_2 species,[48,49] thereby activating the surface for the next half cycle of Ru precursor exposure. Also, the oxygen molecules can serve as a generator of Ru oxide layer as observed at 830 cm^{-1} in Figure 6b by attacking the surface-Ru layer in parallel through a dissociative oxidation. These two functions of the oxygen molecules are closely correlated to each other because Ru oxide layer promotes the CO oxidation reaction. The selective reactivity of bridged CO and terminal CO species on the catalyst has been reported for the oxidation reaction with oxygen molecules.[50] In some cases, the bridged CO is more reactive with O_2 gas than the linearly bonded CO, such as on the $FeO_x/Pt/TiO_2$ catalyst where oxidation reactions are enhanced by adding H_2 gas or water vapor.[49] Even though the Ru/Ru oxide film is not the same as the one mentioned above, both are metal systems that contain an oxide. Oxygen molecules readily react with the bridged CO to produce terminal CO species. We note that if a trace amount of H_2 gas or water vapor was

(44) Cabilla, G. C.; Bonivardi, A. L.; Baltanás, M. A. *Catal. Lett*. **1998**, *55*, 147–156.
(45) Bonelli, B.; Civalleri, B.; Fubini, B.; Ugliengo, P.; Arean, C. O.; Garrone, E. *J. Phys. Chem. B* **2000**, *104*(47), 10978–10988.
(46) Swart, I.; Groot, F.; Weckhuysen, B.; Rayner, D.; Meijer, G.; Fielicke, A. *J. Am. Chem. Soc*. **2008**, *130*, 2126–2127.
(47) Stampfl, C.; Scheffler, M. *Phys. Rev. B* **2002**, *65*, 155417–11.
(48) Bottcher, A.; Niehus, H.; Schwegmann, S.; Over, H.; Ertl, G. *J. Phys. Chem. B* **1997**, *101*(51), 11185–11191.
(49) Kenichi, T.; Masashi, S.; He, H.; Shi, X. *Catal. Lett*. **2006**, *110*, 185–190.
(50) Kenichi, T.; Masashi, S. *Catal. Catal*. **2005**, *47*(6), 418–420.

formed as byproducts, then the conversion reaction would be further facilitated. The high reactivity of the O-rich Ru surface for adsorbed CO oxidation reaction has been well-studied.[51] When terminal CO species are generated from bridged CO species, they become less strongly bound on the O-rich Ru surface than on the metallic Ru surface.[51] Similar results have been reported, emphasizing that the adsorption energy of terminal CO species is reduced upon increasing of oxygen coverage on Ru metal surface.[47] Moreover, the reaction rate of adsorbed CO oxidation on the Ru oxide layer under high pressure of oxygen gas has been reported to be much higher than under low pressure.[51] Therefore, a part of terminal CO would proceed to terminal CO_2 species slowly to complete the oxidation reaction. The same experimental observation was reported on an epitaxial layer of Ru oxide that was formed when the metallic Ru surface was exposed to oxygen molecules.[51] The Ru oxide layer under oxygen gas supply can be modeled to include two kinds of Ru atoms, coordinately unsaturated Ru (active for adsorption), and oxygen-capped Ru (less active for adsorption). Both types of Ru oxide species are believed to participate in oxidation of adsorbed CO to promote the reaction rate on the surface.

As seen in the RBS results of Figure 5, the growth rate is linear after three growth cycles. The growth rate is higher than 1.4 Å/cycle ($\approx 1.0 \times 10^{15}$ atoms/cm^2/ 7.27×10^{22} atoms/cm^3) if we use the Ru atom density of $\sim 1.0 \times 10^{15}$ atoms/cm^2 per cycle from Table 1 and assume that the deposited layer is composed only of metallic Ru. If instead we use the Ru atom density of RuO_2 (3.16×10^{22} atoms/cm^3), the rate is ~3.2 Å/cycle. If the film is composed of a mixture of Ru metallic and Ru oxide, the growth rate would be between about 1.4 and 3.2 Å/cycle. Such growth rates are much higher than previously reported for Ru ALD growth rate using different Ru precursors (~0.5−1.0 Å/cycle).[2,4,13,14] This finding confirms that although the reaction is self-terminated by the formation of bridged CO, it leads to the deposition of more than just one monolayer per cycle. It is also consistent with an inhomogeneous growth, involving agglomeration of Ru into particles and islands, as a complete layer develops. The high rate of film growth is basically due to the fact that the process is not an ALD process, but a process in which formation of terminal CO or CO_2 species takes place on the surface during O_2 pulses instead of removal of ligands from the adsorbed Ru precursor. If the surface is not covered with enough bridged CO species, the surface reaction of Ru precursor would continue at active sites (those that are not yet covered with bridged CO species). These active sites include terminal CO, terminal CO_2, and surface-Ru atoms (including dangling sites generated by desorption of terminal CO_2 species or produced by Ru-precursor reaction) or Ru oxide species[52,53] available on the substrate surface.

3.4. Metallic Property of the Film. To determine the chemical state of the film, the physical nature of the deposited film and the metallic properties of Ru and/or Ru oxide, ex situ XPS measurements were performed. Figure 7 shows the Ru 3d and O 1s core level positions for two different film thicknesses. Curve fitting is carried out with mixed Gaussian−Lorentzian functions for the Ru 3d core level. For the sample deposited with 12 cycles, four peaks are observed in the Ru 3d binding energy region (Figure 7a) at 279.83 and 283.98 eV (pure Ru), and at 280.80 and 284.95 eV (RuO_2). After 24 cycles (Figure 7b), the peaks at 279.92 and 284.07 eV are attributed to pure-Ru film, and those at 280.71 and 284.86 eV to RuO_2.[10,18,54] The two peaks colored in black at 284.7 and 286.5 eV in each figure are associated with carbon. Although the component of the O 1s core level intensity associated with RuO_2 is weak for 12 cycles in Figure 7a,[54] it gains intensity at 529.90 eV for 24 cycles as shown in Figure 7b. These results are consistent with in situ IR data (Figure 6) showing the appearance of a Ru=O stretching band only after 5 cycles.

AFM measurements were performed to investigate the homogeneity and morphology of the films (Figure 8). The films appear grainy and coarse, and the grain size increases with the number of cycles. In addition, the root-mean-square (rms) surface roughness increases from 0.24 nm (12 cycles) to 1.38 nm (24 cycles). These observations suggest that the growth of Ru films occurs via islanding in the early stages of growth, and thereafter continues to develop in an inhomogeneous manner. It is therefore necessary to assess how conductive the films are, particularly after 22 cycles. Information about the film conductivity can be obtained by measuring the broadband IR absorption arising from the electronic response of the free carriers in the film. Figure 9 shows such infrared broadband absorption as a function of film thickness. The absolute absorbance is plotted without any renormalization or background subtraction, which is sometimes employed to study vibrational features. Thus, the increase in broadband absorption indicates that the electronic absorption increases with the number of growth cycles. Initially, the absorbance is stronger in the higher wavenumber region, indicating that electronic scattering dominates, presumably due to high index features (e.g., agglomerated Ru and RuO_2 particles and islands), consistent with formation of an inhomogeneous conducting film. In accordance with AFM results, such scattering is most likely induced by the presence of small Ru patches or grains, characterized by a large (metallic) dielectric function. The large refractive index difference between the silicon substrate and the Ru grains provides the main ingredient for strong Mie scattering.[55] As the average film

(51) Over, H.; Kim, Y. D.; Seitsonen, A. P.; Wendt, S.; Lundgren, E.; Schmid, M.; Varga, P.; Morgante, A.; Ertl, G. *Science* **2000**, *287*, 1474–1476.
(52) Fan, C. Y.; Wang, J.; Jacobi, K.; Ertl, G. *J. Chem. Phys.* **2002**, *114*, 10058–10062.
(53) Wang, J.; Fan, C. Y.; Jacobi, K.; Ertl, G. *J. Phys. Chem. B* **2002**, *106*, 3422–3427.
(54) Chen, W.; Zhang, M.; Zhang, D. W.; Ding, S.-J.; Tan, J. J.; Xu, M.; Qu, X.-P.; Wang, L. K. *Appl. Surf. Sci.* **2007**, *253*(8), 4045–4050.
(55) Stratton, J. A. In *Electromagnetic Theory*; McGrow-Hill: New York, 1941.

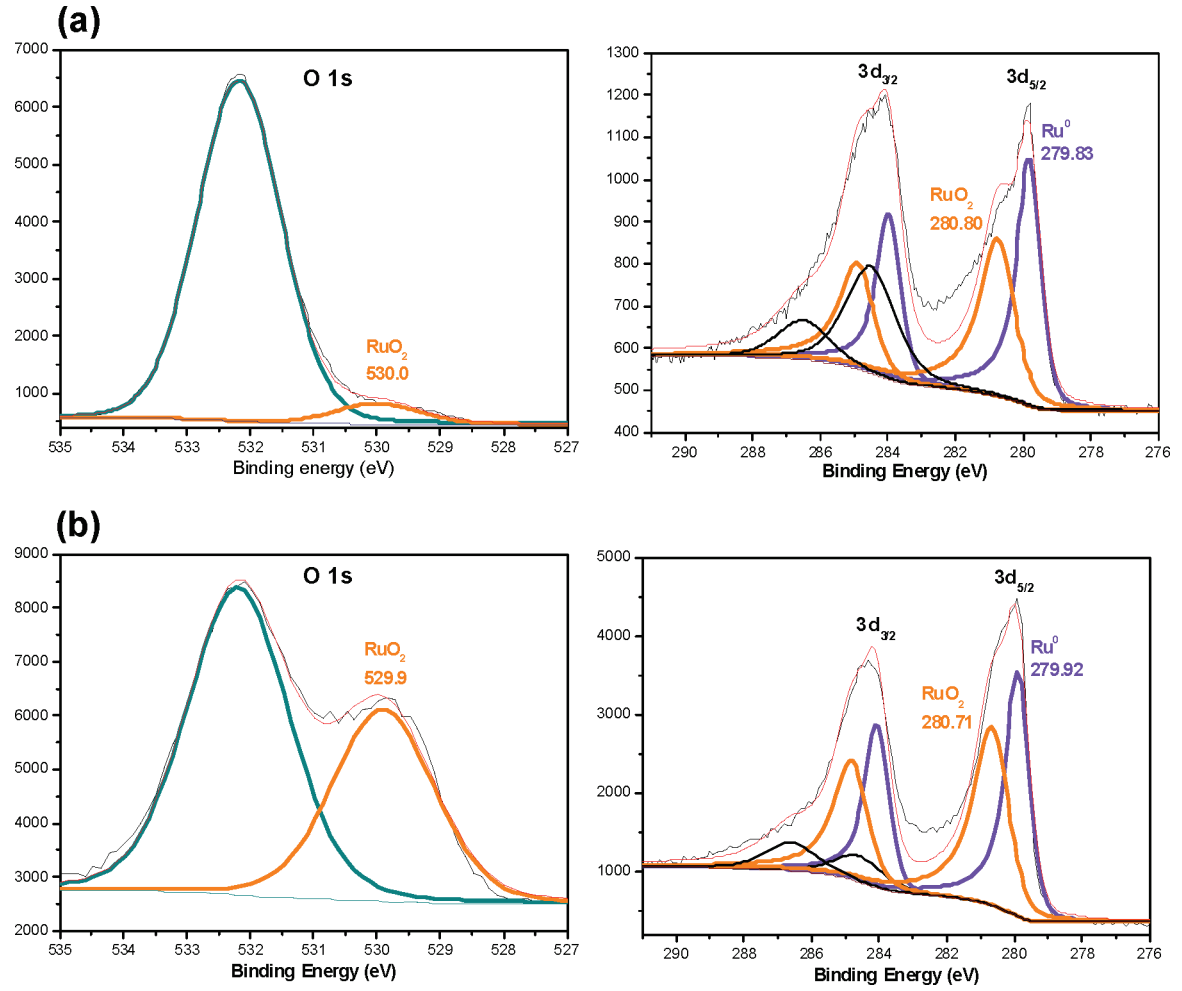

Figure 7. XPS spectra at O 1s and Ru 3d core level for films deposited on H/Si (111) at 300 °C: (a) after 12 cycles and (b) after 24 cycles.

thickness increases, particularly after 22 cycles shown in Figure 9, the background absorption displays a qualitative change characterized by a large increase in absorption at lower wavenumbers. Such dependence is characteristic of free electron absorption, also termed Drude absorption, which would be observed when the grains coalesce to form a continuous film.[56] Although the films are rather far from being homogeneous, flat and smooth (see AFM pictures in Figure 8), the free electron absorption is now dominant over scattering, in this film system, after deposition of 24 cycles, confirming that the films are at least continuous.

It is unfortunately not possible to go beyond ~30 cycles because the sample becomes opaque due to free carrier absorption. The transmission is too weak to perform meaningful IR absorption studies. To investigate the properties of thicker films, a separate ALD system needs to be used, as described in the next section.

3.5. Thicker Ru Film Properties. In the above study, the exposure conditions involve a 5 s pulse (with low pumping speed) and 25 s static exposure (no pumping) as described earlier. With only a 5 s dynamic exposure, typical of ALD growth, the surface reaction does not reach completion until there is clearly precursor decomposition (above 300 °C). Also, the process is not self-terminated at 300 °C, the temperature at which the film is grown. For those reasons, the longer (unconventional) exposure cycle has been used for this study.

For completeness, we present data recorded on thicker films grown using conventional ALD growth parameters (1 s pulse length, dynamic exposures). Specifically, the $Ru(Cp)(CO)_2Et$ precursor was vapor drawn at 90 °C (1 s pulse, no carrier gas) and the O_2 pulse (1 s, 10 sccm) were separated by 9 s N_2 purge (10 sccm, system at 100 mTorr) and the sample was kept at 300 °C. Under these conditions, there is a substantial incubation period on H-terminated surfaces, leading to an overall growth rate of ~0.8 Å/cycle. For comparison, growth in similar conditions on oxidized silicon yields ~0.9 Å/cycle.

Figure 10 shows X-ray photoemission core-level spectrum of Ru 3d of a 45-nm thick Ru film grown as described above, obtained after removing of the oxidized surface region by sputtering. The Ru 3d binding energy at 280.1 eV is consistent with metallic Ru^0 and the amount of oxygen is less than 1%. The films are therefore of reasonable quality. An X-ray diffraction analysis reveals that the film structure is hexagonal close packed (hcp)

(56) Tolstoy, V. P.; Chernyshova, I. V.; Skryshevsky, V. A. In *Handbook of Infrared Spectroscopy of Ultrathin Films*; John Wiley and Sons: New York, 2003.

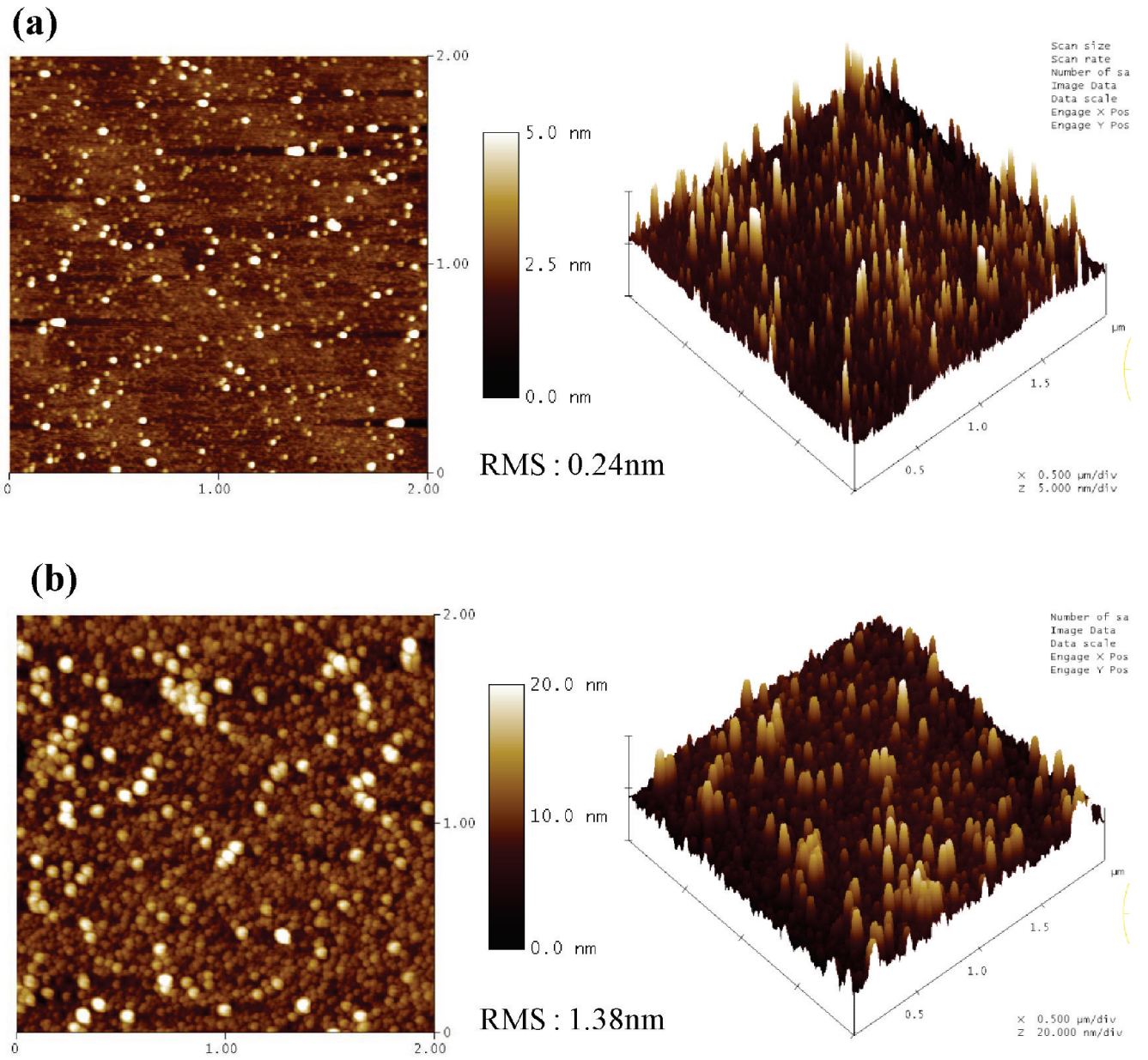

Figure 8. AFM images of films on H/Si (111) at 300 °C: (a) after 12 cycles and (b) after 24 cycles.

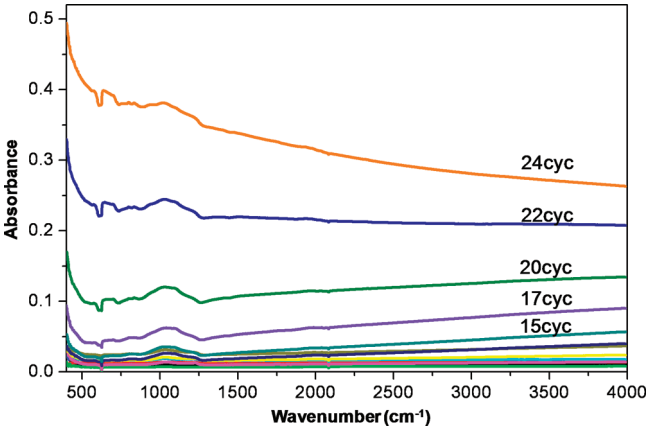

Figure 9. IR absorption spectra for the metallic growth of film deposited on H/Si (111) at 300 °C, referenced to the initial H/Si (111) without baseline correction or shift.

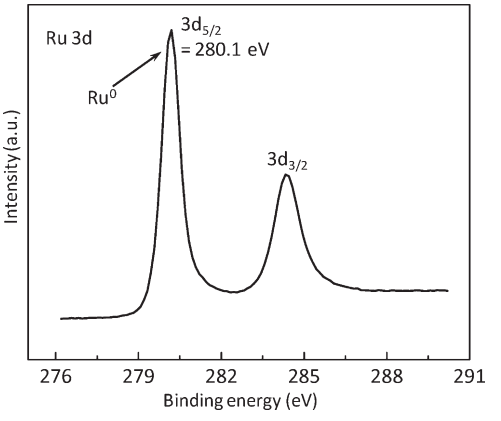

Figure 10. X-ray photoemission spectrum of Ru 3d of 45-nm thick ALD grown Ru film with alternating 1 s $Ru(Cp)(CO)_2Et$ and 1 s O_2 pulsing, separated by a 9 s N_2 purge.

expected for pure Ru. A four point probe study shows that for films grown with 430−600 cycles the resistivity is ~18 $\mu\Omega$ cm.

This study indicates that Ru films of reasonable quality can be grown using this new precursor under conditions that are typical of ALD growth. However, it is clear that the growth is not self-limited through a conventional ALD process but simply terminated by a short pulse length.

4. Conclusions

The growth of Ru/RuO_2 films using an atomically controlled layer deposition method was performed with a newly synthesized precursor $Ru(Cp)(CO)_2Et$ and O_2 gas. The parameters for saturated growth were determined for the initial growth: sample temperature (300 °C), precursor pulse length (5s for Ru precursor dosing and 25s duration without pumping and 2s for O_2) and precursor gas pressure (1.1 Torr using N_2 carrier gas). Ligand exchange is initially observed in the IR absorption spectra after each half cycle. For the first two cycles, the growth rate is low. Thereafter, the growth rate increases and becomes linear after 3 cycles and are higher (~1.4−3 Å/cycle) than typical ALD growth. Under our experimental growth conditions, the resulting films are composed of a mixture of both Ru and RuO_2. While the initial growth is dominated by the deposition of unoxidized Ru, RuO_2 is formed after a few growth cycles and becomes comparable to Ru metal in later cycles, also displaying a linear growth rate. IR measurements show that terminal CO, bridged CO and terminal CO_2 species are formed on the surface, and found to play crucial roles for film growth. In particular, the bridged CO species acts as a surface reaction terminator and O_2 gas as an activator. The increased coverage of bridged CO species during the Ru precursor cycle blocks the activity of Ru precursor on the surface and therefore terminates the film growth, whereas O_2 gas exposure activates the surface by converting bridged CO species to terminal CO or terminal CO_2 species on the surface. The terminal CO_2 species is labile, so it can readily desorb from the surface. Exposing the surface to O_2 gas also generates a Ru oxide layer (presumably by dissociative oxidation), which may contribute to the oxidation of adsorbed CO species on the surface.

As the average film becomes thicker, particularly after 22 cycles, there is evidence for electronic absorption in broadband IR absorption spectra, with increasing absorption on the lower wavenumber side. Such dependence is characteristic of a continuous metallic film characterized by free electron absorption (Drude absorption), which is possible when the metallic grains coalesce. Overall, the results show a reasonable agreement with the amount of Ru and RuO_2 estimated from RBS and XPS measurements, which also show the coexistence of both Ru and RuO_2 phases with the appearance of RuO_2 at the later stages of the growth.

In contrast to films grown by using saturation conditions, films grown using conditions more typical for ALD growth on substrates at 300 °C lead to a slower growth (~0.8 Å/cycle) of metallic Ru. Under these conditions, the growth is not self-limited and therefore not purely an ALD growth.

Acknowledgment. Funding for this work was provided by SAFC Hitech and by the National Science Foundation (Grant CHE-0827634).